Mon. Not. R. Astron. Soc. **393,** 872–884 (2009) doi:10.1111/j.1365-2966.2008.13874.x

CRASHα: coupling continuum and line radiative transfer

M. Pierleoni,* A. Maselli and B. Ciardi

Max-Planck-Institut für Astrophysik, Karl-Schwarzschild-Strasse 1, D-85748 Garching b. Muenchen, Germany

Accepted 2008 August 22. Received 2008 August 1; in original form 2007 December 7

ABSTRACT

In this paper we present CRASHα, the first radiative transfer code for cosmological application that follows the parallel propagation of Lyα and ionizing photons. CRASHα is a version of the continuum radiative transfer code CRASH with a new algorithm to follow the propagation of Lyα photons through a gas configuration whose ionization structure is evolving. The implementation introduces the time evolution for Lyα photons (a feature commonly neglected in line radiative transfer codes) and, to reduce the computational time needed to follow each scattering, adopts a statistical approach to the Lyα treatment by making extensive use of pre-compiled tables. These tables describe the physical characteristics of a photon escaping from a gas cell where it was trapped by scattering as a function of the gas temperature/density and of the incoming photon frequency. With this statistical approach we experience a drastic increase of the computational speed and, at the same time, an excellent agreement with the full Lyα radiative transfer computations of the code MCLYα. We find that the emerging spectra keep memory of the ionization history which generates a given ionization configuration of the gas and, to properly account for this effect, a self-consistent joint evolution of line and ionizing continuum radiation as implemented in CRASHα is necessary. A comparison between the results from our code and from Lyα scattering alone on a fixed H I density field shows that the extent of the difference between the emerging spectra depends on the particular configuration considered, but it can be substantial and can thus affect the physical interpretation of the problem at hand. These differences should furthermore be taken into account when computing the impact of the Lyα radiation on e.g. the observability of the 21-cm line from neutral hydrogen at epochs preceding complete reionization.

Key words: line: profiles – radiative transfer – methods: numerical.

1 INTRODUCTION

The detection of Lyα lines from local and distant objects has always been of great importance in astrophysics. It has been extensively used as indicator of redshift, as a measurement of the star formation activity of galaxies and as a probe of their internal structure. In the last few years an increasing interest has been devoted to the search of Lyα emitters (LAEs) at high redshift, which are expected to be characterized by a strong Lyα emission (Partridge & Peebles 1967), but significantly attenuated by dust absorption. In fact, it has been necessary to wait for dedicated large programmes of deep narrow band searches like the Large Area Lyman Alpha (LALA) and the Subaru Deep Field survey to detect a significant number of emission galaxies at high redshift (e.g. Stern et al. 2005; Iye et al. 2006) and to get complete spectroscopic samples of LAEs at redshift $z = 4.5, 5.7$ and 6.5 (e.g. Hu et al. 1998; Rhoads & Malhotra 2001; Kodaira et al. 2003; Hu et al. 2004; Taniguchi et al. 2005; Kashikawa et al. 2006; Dawson et al. 2007; Murayama et al. 2007). Strong lensing magnification has been necessary to move the detection frontiers even further, with several candidates currently observed up to $z \simeq 10$ (e.g. Pelló et al. 2007; Stark et al. 2007).

The intense activity reported above is explained by the great interest in using LAEs as cosmological probes: LAEs are in fact the objects with the highest known z and can be used to study large-scale structures and galaxy formation in the high-redshift universe. Number counts, together with the statistics of line shapes, are extremely powerful observables from which inferring important information about e.g. the properties of the intergalactic medium (IGM) and the reionization era (e.g. Hu et al. 2002; Rhoads et al. 2003; Stern et al. 2005), the photoionization processes and UV photon production (e.g. Stark et al. 2007), the tomography of neutral gas, gas velocity field and star formation activity (e.g. Kodaira et al. 2003). This predicting power relies on the fact that the Lyα line is shaped inside the galaxy interstellar medium and at high redshift is also affected by the IGM opacity, which becomes non-negligible to Lyα photons at $z \gtrsim 6$ (Fan et al. 2006).

*E-mail: mpierleoni@mpa-garching.mpg.de

Emission of Lyα photons from high-redshift sources has also an impact on the detectability of 21-cm line from neutral hydrogen in the IGM. At high redshift, the Wouthuysen–Field effect (Wouthuysen 1952; Field 1958, 1959) is in fact extremely efficient in decoupling the spin temperature of the gas, T_s, from the cosmic microwave background (CMB) temperature, T_{CMB}, allowing the 21-cm signal to be visible either in absorption or in emission. Fluctuations in the Lyα flux, due both to inhomogeneous distribution of the Lyα radiation sources and to the scattering in the wings, can modify the expected signal (e.g. Barkana & Loeb 2005; Chuzhoy & Zheng 2007; Semelin, Combes & Baek 2007; Chen & Miralda-Escudé 2008), at least as long as a strong Lyα background is not established and the radiation intensity reaches a saturation level (e.g. Ciardi & Madau 2003; Ciardi & Salvaterra 2007). For these reasons, it is important to follow the propagation of Lyα photons rather than assume a homogeneous background as it is generally done.

Due to the resonant nature of the Lyα line propagation, a self-consistent and detailed treatment of the line radiation transfer is required in order to model properly how Lyα radiation affects the IGM, as well as to understand how different physical processes shape the spectral features of LAEs. As a consequence of the great interest in this field, several semi-analytic and numerical studies of the Lyα radiative transfer have followed the first pioneering papers on the subject (Osterbrock 1962; Avery & House 1968; Adams 1972; Harrington 1973; Neufeld 1990). Analytic solutions have been derived only for few simple geometrical gas configurations: static plane parallel slabs including dust (Neufeld 1990), static uniform sphere (Dijkstra, Haiman & Spaans 2006) and uniform gas with pure Hubble flow around a steady Lyα source (Loeb & Rybicki 1999). Given the difficulties in the treatment of radiative transfer though, also the numerical approaches developed so far, mostly based on Monte Carlo techniques, have been in most cases specifically designed for particular physical configurations and problems: 1D dusty and optically thick media (Ahn, Lee & Lee 2000, 2001); 3D arbitrary distribution of dustless gas with arbitrary bulk velocity field (Zheng & Miralda-Escudé 2002); spherically symmetric collapsing gas clouds (Dijkstra et al. 2006); Lyα scattering off opaque, dusty and moving clouds (Hansen & Oh 2006); Hubble-like expansion flows of neutral gas (Loeb & Rybicki 1999; Kobayashi & Kamara 2004). Other codes have been specifically designed for studying LAEs and Lyα pumping in a cosmological context (Gould & Weinberg 1996; Cantalupo et al. 2005; Tasitsiomi 2006; Semelin et al. 2007). Verhamme, Schaerer & Maselli (2006, hereafter VSM06) have developed a general-purpose 3D Lyα radiation transfer code applicable to dusty media with arbitrary geometries and velocity fields.

So far analytical, semi-analytical as well as numerical studies perform the Lyα radiative transfer as a post-process calculation by assuming a fixed ionization structure of the gas through which it propagates, while none of them has tackled the Lyα radiative transfer problem by taking into account the effect of an evolving ionization configuration. Nevertheless, as we show in the following, this approximation results to be a poor one for some applications of interest, in particular for cosmological studies at high redshift, but also when modelling the Lyα emission from young galaxies.

In this paper we present CRASHα, a new radiative transfer scheme which, for the first time in the literature, follows simultaneously the propagation of Lyα and ionizing radiation self-consistently. This allows us to investigate the effects of evolving ionization configurations on the propagation of Lyα radiation and on the shaping of the line emerging from single objects. The impact of an evolving ionization structure can in fact be significant and needs to be taken into account: the large cross-section of Lyα photons makes propagation dominated by resonant scattering with H I atoms and the random-walk-like nature of the process makes the characteristic time for Lyα photon propagation much larger than the one for ionizing radiation. If an ionizing continuum changes the ionization of the gas through which the Lyα photon is propagating, the amount of scattering suffered by the line photons before escaping will depend on the ionization history of the system. In this case, a joint treatment of both line and continuum transfer is needed to study the alterations in the Lyα spectrum occurring during the evolutionary stages of the ionized regions.

The code presented in this paper is the first step in this direction. CRASHα has been implemented as an extension of the 3D ray-tracing radiative transfer code for ionizing radiation CRASH (Ciardi et al. 2001; Maselli, Ferrara & Ciardi 2003; Maselli & Ferrara 2005; Maselli, Ciardi & Kanekar, in preparation), by developing a new independent algorithm which follows the path of line photons in time and space. As described in details in the following, this new algorithm makes extensive use of pre-compiled tables which have been derived by using the line transfer code MCLYα (VSM06) and allows us to compute in an extremely efficient way the path of line photons in arbitrary 3D gas distributions.

The paper is structured as follows. Section 2 is dedicated to a brief overview of CRASH and MCLYα, while in Section 3 we describe the new method. Some validation tests are shown in Section 4. In the last section we present a summary of the paper.

2 CRASH AND MCLY α

In this section we give a brief description of the codes CRASH and MCLYα for the sake of providing a proper background for the description of CRASHα given in Section 3. A more detailed description of the two codes is already in the literature: the details of CRASH implementation are given mostly in Maselli et al. (2003), with updates on a new scheme for the background radiation field given in Maselli & Ferrara (2005) and on the latest version of the code in Maselli et al. (in preparation). MCLYα algorithm is fully described in VSM06. Note that some nomenclature has been changed for clarity.

2.1 CRASH: continuum radiative transfer

CRASH is a 3D ray-tracing radiative transfer code based on Monte Carlo (MC) techniques that are used to sample the probability distribution functions (PDFs) of several quantities involved in the calculation, e.g. spectrum of the sources, emission direction, optical depth. The MC approach and the code architecture assure a great flexibility in the application to a wide range of astrophysical problems and allow additional physics to be easily added with a minimum effort.

The algorithm follows the propagation of the ionizing radiation through an arbitrary H/He static density field and at the same time computes the variations in temperature and ionization state of the gas. Both multiple point sources, located arbitrarily in the box, and diffuse radiation (e.g. the ultraviolet background or the radiation produced by H/He recombinations) can be accounted for. In this paper we neglect the treatment of any background radiation for simplicity.

The energy emitted by point sources in ionizing radiation is discretized into photon packets, beams of ionizing photons, emitted at regularly spaced time intervals. More specifically, the total energy radiated by a single source of luminosity L_s, during the total simulation time, t_{sim}, is $E_s = \int_0^{t_{sim}} L_s(t_s)\,dt_s$. For each source, E_s is

distributed in $N_{\rm p}$ photon packets, emitted at the source location at regularly spaced time intervals, $\mathrm{d}t = t_{\rm sim}/N_{\rm p}$. The time resolution of a given run is thus fixed by $N_{\rm p}$ and the time evolution is marked by the packet emission: the jth packet is emitted at time $t^j{}_{\rm em,c} = j\mathrm{d}t$, with $j = 0, \ldots, (N_{\rm p} - 1)$. Thus, the total number of emissions of continuum photon packets is $N_{\rm em,c} = N_{\rm p}$. In its latest version (Maselli et al., in preparation), the code allows for polychromatic packets whose content consists of photons distributed in various frequency bins which are populated according to the spectral shape assigned to the source.

The emission direction of each photon packet is assigned by MC sampling the angular PDF characteristic of the source. The propagation of the packet through the given density field is then followed and the impact of radiation–matter interaction on the gas properties is computed on the fly. Each time the packet pierces a cell i, the cell optical depth for ionizing continuum radiation, $\tau^i_{\rm c}$, is estimated summing up the contribution of the different absorbers (H I, He I, He II). As the probability for a single photon to be absorbed in such a cell is

$$P(\tau^i_{\rm c}) = 1 - \mathrm{e}^{-\tau^i_{\rm c}}, \tag{1}$$

the number of photons absorbed in the cell i is the fraction $P(\tau^i_{\rm c})$ of packet content when entering the cell. In the polychromatic implementation, the same argument applies to the number of photons contained in each single-frequency bin. The trajectory of the packet is followed until its photon content is extinguished or, if continuum boundary conditions are not assumed, until it exits the simulation volume.

The time evolution of the gas physical properties (ionization fractions and temperature) is computed solving in each cell the appropriate discretized differential equations each time the cell is crossed by a packet. The reader is referred to Maselli et al. (2003) and Maselli et al. (in preparation) for more details.

2.2 MCLYα: line radiative transfer

MCLYα is a numerical scheme for Lyα line radiative transfer, whose implementation is based on the basic structure of CRASH. MCLYα in fact uses the same MC sampling and ray-tracing techniques and it allows for arbitrary 3D hydrogen plus dust density distributions, as well as for arbitrary ionization, temperature and velocity fields.

There are three physical processes, included in the code, which affect the propagation of the line radiation: Lyα line scattering, dust absorption and dust scattering. For the sake of simplicity, in this paper we concentrate solely on the effect of Lyα line scattering and we defer the treatment of the interaction between radiation and dust to future work. Here we describe the basic structure of the algorithm in the absence of dust. For a more complete and accurate description the reader is referred to the original paper (VSM06).

Lyα is the strongest H I transition, for which the cross-section assumes large values at frequencies near the line centre, $\nu_0 = 2.466 \times 10^{15}$ Hz. It is convenient to introduce the frequency shift

$$x = \frac{\nu - \nu_0}{\Delta\nu_{\rm D}}, \tag{2}$$

where $\Delta\nu_{\rm D} = (V_{\rm th}/c)\ \nu_0$ corresponds to the Doppler frequency width and $V_{\rm th}$ is the velocity dispersion of the Maxwellian distribution describing the thermal motions, i.e. $V_{\rm th} = (2k_{\rm B}\,T/m_{\rm H})^{1/2} = 12.85\,T_4^{1/2}\,\mathrm{km\,s^{-1}}$, with T_4 being the gas temperature in units of 10^4 K. The other symbols have the usual meaning. Here we neglect turbulent motions, but the option is available for their inclusion.

The Lyα line radiation field is reproduced by emitting photons from each source and by following their path through the assigned gas distribution until they escape from the simulation box. The location of interaction between the Lyα photons and the gas is determined by MC sampling the PDF for the line optical depth a photon crosses before being scattered, $P(\tau_{\rm l}) = 1 - \mathrm{e}^{-\tau_{\rm l}}$. In other terms, the location of interaction is determined as the cell at which the total optical depth from the emission location, $\tau_{\rm l} = \sum_i \tau^i_{\rm l}$ (where the sum extends over all the cells crossed by the photon), becomes larger than $\tau_{\rm scatt} = -\ln(1 - \xi)$, where ξ is a random number extracted in the interval [0:1[.

The next step, after assessing the absorption location, is to determine the photon frequency following a scattering with a hydrogen atom. To do this, the code first converts the frequency of the photon from the external (observer) frame, $\nu_{\rm obs}$, to the one comoving with the fluid, $\nu_{\rm com}$, performing a Lorentz transformation:

$$\nu_{\rm com} = \nu_{\rm obs}\left(1 - \frac{\boldsymbol{k}_{\rm in}\cdot\boldsymbol{V}}{c}\right), \tag{3}$$

where $\boldsymbol{k}_{\rm in}$ is the incoming photon direction and $\boldsymbol{V}$ the bulk velocity of H atoms. Due to the thermal motion of H atoms, scattering in the fluid comoving frame is not perfectly coherent. Within the comoving framework[1] and neglecting the recoil effect, partially coherent scattering can be described with a simple relation between the incoming, $x_{\rm in}$, and the outgoing, $x_{\rm out}$, frequency (Dijkstra et al. 2006):

$$x_{\rm out} = x_{\rm in} - \frac{\boldsymbol{V}_{\rm a}\cdot\boldsymbol{k}_{\rm in}}{V_{\rm th}} + \frac{\boldsymbol{V}_{\rm a}\cdot\boldsymbol{k}_{\rm out}}{V_{\rm th}}. \tag{4}$$

In the above equation $\boldsymbol{V}_{\rm a}$ is the atom velocity, while $\boldsymbol{k}_{\rm in}$ and $\boldsymbol{k}_{\rm out}$ are, respectively, the incoming and outgoing propagation directions. The code can model both isotropic and dipolar angular redistribution; in this paper we use only the isotropic redistribution and sample randomly the outgoing propagation direction.

Once a new direction and frequency are assigned to the scattered photon, a new random ξ is extracted to determine the next scattering location.

This scheme is repeated until the photon escapes the simulation volume.

3 CRASH α: COMBINING CONTINUUM AND LINE TRANSFER

In this section we describe CRASHα, the first numerical scheme which combines the treatment of continuum and line transfer radiation. As mentioned in Section 1, the algorithm has been developed as an extension of CRASH, which provides the treatment of the ionizing radiation as described in the previous section and references therein. The extension indeed consists in a new algorithm developed to follow the propagation of Lyα photons through a given gas configuration while it is changed by ionizing radiation. In fact, although the continuum photon propagation proceeds undisturbed by the Lyα radiation field, Lyα radiative transfer is strongly affected by the change in the ionization state of the gas.

In order to perform the coupling, it is necessary to introduce the time evolution for Lyα propagation, a feature commonly neglected in line radiative transfer codes like MCLYα. This is a crucial aspect because, due to the resonant scattering nature of Lyα transfer in a neutral medium, Lyα radiation can remain trapped for a substantial

[1] Here and in the following we omit the comoving suffix for the sake of keeping an easily readable notation.

fraction of the simulation lifetime before being able to propagate away from its emission site, while the propagation time of the ionization front can be much shorter. Thus, the change in the degree of ionization affects the propagation of the Lyα photons, while the latter induces no back reaction on the gas. Note that, although Lyα photons, via scattering, can transfer some of their energy to the gas and heat it, in typical situations the effect is negligible and thus such heating is not generally included in Lyα radiative transfer codes. We defer the investigation of this issue in more detail to future work.

To correctly model the simultaneous propagation of the two radiations a combined approach is needed. This is a challenging task because of the very different nature of continuum and line transfer, in terms of e.g. their path (straight line versus random walk) and time-scales (see discussion above). The above differences are reflected also in the numerical implementation of line and continuum radiative transfer. For example, while in the case of ionizing radiation the time needed for a photon packet to travel a given distance does not depend sensibly on the physical properties of the gas but only on the physical distance crossed, the propagation of Lyα photons is very sensitive to the ionization state of the gas and extreme configurations can be faced, in which the Lyα photons scatter for the entire simulation time trapped in few cells without exiting the simulation volume.

As the ionizing radiation scheme has not been modified, it will not be discussed further and in the following we will focus on describing the details of the line transfer part of the algorithm.

The Lyα radiation is discretized in a large number of photons whose emission and propagation is dictated by the time-scale attached to the ionizing radiation evolution. In this way we are able to model the change in the Lyα propagation due to the variations in the gas ionization state. To correctly model the propagation of Lyα photons we need to follow every single scattering. As this would require a very large computational time, we use a statistical approach to the Lyα treatment. We have compiled 1085 tables by running MCLYα, in order to describe the physical characteristics of a photon after a scattering depending on the temperature and density of the gas and on the incoming photon frequency (see Appendix A). The following part of this section is dedicated to a description of the various steps of the implementation.

3.1 Emission of Lyα photons

Every Lyα emission is characterized by the generation of $N_{\gamma,\mathrm{l}}$ Lyα line photons emitted at the same time, $t^i_{\mathrm{em,l}}$. The parameter $N_{\gamma,\mathrm{l}}$ is chosen to optimize the resolution and the code performance. The code allows for two different methods for photon emission. In the first method the emission is regularly spaced in time as in the continuum emission. If, as in Section 2.1, we define $N_{\mathrm{em,l}}$ as the total number of emissions of line photons, in this case:

$$t^i_{\mathrm{em,l}} = i\,\frac{t_{\mathrm{sim}}}{N_{\mathrm{em,l}}}, \tag{5}$$

with $i = 0, \ldots, (N_{\mathrm{em,l}} - 1)$.

An alternative criterion for the emission follows the evolution of the ionization structure. In this case the emission time, $t^i_{\mathrm{em,l}}$, is linked to the volume-averaged H ionization fraction, $\chi_{\mathrm{H\,II,em}}$, and Lyα photons are emitted at the time $t^i_{\mathrm{em,l}}$ when

$$\chi^i_{\mathrm{H\,II,em}} = i\,\Delta\chi_{\mathrm{H\,II}}. \tag{6}$$

$\Delta\chi_{\mathrm{H\,II}} = 1/N_{\mathrm{em,l}}$ is the chosen H II fraction variation in the gas and i is an integer that covers values between 0 and $N_{\mathrm{em,l}} - 1$. While in the first formulation a constant Lyα emission rate is assured, in this case the emission rate is higher when the ionization state of the gas changes faster. In order to reproduce a constant emissivity even in the second formulation, we assign a weight to each photon emitted at the ith step: $w^i_{\mathrm{ph}} = (t^i_{\mathrm{em,l}} - t^{i-1}_{\mathrm{em,l}})/t_{\mathrm{sim}}$. When an Lyα spectrum is built, each photon contributes according to its weight. This allows us to modulate the emission of Lyα photons based on the change of the ionization degree (and thus to better sample the effect of ionization on Lyα scattering) and at the same time to have a constant Lyα photon rate.

In the following tests the emission is assumed to be isotropic, but it is always possible to account for an arbitrary angular PDF.

Every emitted Lyα photon k ($k \in [1, N_{\gamma,\mathrm{l}} \times N_{\mathrm{em,l}}]$) is described by its frequency in the comoving frame $x_{\mathrm{in},k}$ (in this case we assume a monochromatic spectrum with $x_{\mathrm{in},k} = 0$, but a different spectrum can be used), position $\boldsymbol{p}_k$ (which coincides with the source location), direction of propagation $\boldsymbol{k}_{\mathrm{in},k}$, optical depth at which the scattering takes place $\tau_{\mathrm{scatt},k}$ (as defined in Section 2.2) and a characteristic time $t_{\mathrm{ch},k} = t^i_{\mathrm{em,l}}$ that is used to evolve the photon along the simulation timeline (see next section). At any step of the simulation the kth photon is always described by the quantities $(x_{\mathrm{in}}, \boldsymbol{p}, \boldsymbol{k}_{\mathrm{in}}, \tau_{\mathrm{scatt}}, t_{\mathrm{ch}})$, where the index k has been omitted for clarity. In the following, we will always omit it.

3.2 Propagation of Lyα photons

In Section 2.1 we have seen how the physical time of the simulation is driven by the emission of packets of ionizing radiation discretized in time units, dt. We are interested now to link the propagation of an Lyα photon to this timeline.

Let us assume that an ionizing photon packet has been emitted at $t^j_{\mathrm{em,c}}$, that the physical state of the gas has been evolved between $t^j_{\mathrm{em,c}}$ and $t^{j+1}_{\mathrm{em,c}}$, and that an Lyα photon is emitted at the same time $t^i_{\mathrm{em,l}} = t^j_{\mathrm{em,c}}$; then its characteristic time is assigned the value $t_{\mathrm{ch}} = t^i_{\mathrm{em,l}}$. The propagation of the Lyα photon along the direction $\boldsymbol{k}$ is followed between t_{ch} and $t^{j+1}_{\mathrm{em,c}}$, and the line optical depth encountered along the path, τ_{l}, is calculated as described in Section 2.2. In each cell crossed by the photon we check if a scattering takes place, i.e. if τ_{l} becomes larger than τ_{scatt}. If there is no scattering, we follow the propagation until $t^{j+1}_{\mathrm{em,c}}$ and at this point we store the photon's frequency x_{in}, the updated position $\boldsymbol{p} = \boldsymbol{p} + (c\mathrm{d}t)\boldsymbol{k}$, and characteristic time $t_{\mathrm{ch}} = t^{j+1}_{\mathrm{em,c}}$. Propagation direction $\boldsymbol{k}_{\mathrm{in}}$ and optical depth for scattering τ_{scatt} remain unchanged. This information will be used to follow the photon evolution in the next time unit. We define this photon as 'active', in the sense that it is not trapped by scattering inside a cell but will resume its propagation in the next time unit.

Let us consider now the case in which the photon scatters during the time unit. Unlike MCLYα, this code does not follow every scattering inside the cell, but determines the properties of the outgoing photon by interpolation of pre-compiled tables (see Appendix A). Once the location of the scattering is identified within a cell, around it we build a new, smaller cell with length equivalent to the shortest distance between the scattering's location and the boundary of the cell. The physical and dynamic gas conditions are the ones of the original cell. As the tables are built with photons that scatter in the centre of a cell, the above procedure removes the dependence on the position of the incoming photon. Given the gas temperature, T_{cell}, the line optical depth, τ_{cell}, of the newly built cell, and the frequency, x_{in}, of the incoming photon, a linear interpolation of the tables is performed to obtain the distribution of frequencies of the outgoing photon, x_{out}, and of the time interval that the photon is expected to spend inside the cell due to scattering, t_{scatt}. From these

distributions the code extracts the values for $x_{\rm out}$ and $t_{\rm scatt}$ that will be assigned to the photon. This approach allows for a tremendous gain in computational speed by adopting a statistical description of the scatterings that occur to the photon inside a cell, without following each one individually. The characteristic time is updated as $t_{\rm ch} = t_{\rm ch} + t_{\rm scatt}$. If $t_{\rm ch} > t^{j+1}_{\rm em,c}$ the photon is put in a 'stand-by' mode and its propagation is resumed (with a new $\tau_{\rm scatt}$) only when the simulation time becomes larger than $t_{\rm ch}$.

The procedure described above is repeated for (i) all the Lyα photons emitted at $t^{j}_{\rm em,l}$, (ii) all the Lyα photons 'active' at $t^{j}{}_{\rm em,c}$ and (iii) all the Lyα photons that exit the 'stand-by' mode in this time unit. Then, a new ionizing photon packet is emitted at $t^{j+1}_{\rm em,c}$ and after it has been evolved up to $t^{j+2}_{\rm em,c}$ the Lyα cycle starts again: all the 'active' photons are evolved from $t^{j+1}_{\rm em,c}$ to $t^{j+2}_{\rm em,c}$; if there are 'stand-by' photons with $t^{j+1}_{\rm em,c} < t_{\rm ch} < t^{j+2}_{\rm em,c}$ they are turned into 'active' photons and evolved until $t^{j+2}_{\rm em,c}$; if new Lyα photons are emitted in this time unit they as well are evolved until $t^{j+2}_{\rm em,c}$.

If the ionizing radiation crosses a cell in which an Lyα photon is trapped by scattering, the change in the physical conditions of the cell should be taken into account, as this affects the characteristics of the outgoing photon. To include this effect, we use tables which give the time evolution of the frequency distribution of photons trapped in a cell as a function of the same input parameters $x_{\rm in}, \tau_{\rm cell}, T_{\rm cell}$. As an example, let us assume that an Lyα photon scatters in a cell at $t_{\rm s,0}$ and that the time at which it exits the 'stand-by' mode is $t_{\rm ch} = t_{\rm s,2}$. If the ionizing radiation crosses that cell at a time $t_{\rm s,1}$ such that $t_{\rm s,0} < t_{\rm s,1} < t_{\rm s,2}$, the physical conditions in the cell change. To take into account the effect on $x_{\rm out}$ and $t_{\rm scatt}$, CRASHα proceeds as follows:

(i) it computes how much time the photon spent in the cell, $t_{\rm s,1} - t_{\rm s,0}$;

(ii) it samples the distribution of frequencies at that time, interpolating the tables mentioned above;

(iii) it extracts a new frequency, $x_{\rm in,1}$, and recalculates $x_{\rm out}$ and $t_{\rm scatt}$ using the values $T_{\rm cell}(t_{\rm s,1}), \tau_{\rm cell}(t_{\rm s,1})$ modified by the ionizing radiation and $x_{\rm in,1}$.

3.3 Spectrum of Lyα photons

When photons exit the simulation box, their frequencies are collected to calculate the outgoing time-integrated spectrum. As discussed in Section 3.1, each photon is counted according to its weight. To show the probability distribution of the outgoing Lyα radiation, spectra are normalized to the sum of all weights. The profile of the final spectrum strongly depends on the choice of the integration time. To build a spectrum we define an initial, $t^{l}_{\rm out}$, and a final, $t^{l+1}_{\rm out}$, time. All the photons that escape from the box in the interval $]t^{l}_{\rm out};t^{l+1}_{\rm out}]$ will contribute to the spectrum of the source. At the next output, all the photons collected in the interval $]t_{l+1\rm out};t^{l+2}_{\rm out}]$ will be used to build the spectrum. This procedure is followed until the end of the simulation. As in the case of the emission described in Section 3.1, the spectra can be produced regularly spaced in time or linked to the evolution of the ionization structure. Thus, the time of the outputs is regulated by equations (5) and (6), where $t^{i}_{\rm em,l}$ and $N_{\rm em,l}$ are replaced by $t^{l}{}_{\rm out}$ and $N_{\rm out}$, respectively.

Spectra can also be built by choosing a pre-determined line of sight.

4 RESULTS

In this section we perform tests for the parallel propagation of ionizing and Lyα radiations, which show how the evolution of the ionization structure alters the Lyα spectra of the outgoing radiation. All the tests have the same initial conditions, unless stated otherwise. We use a simulation box of 30 pc on a side, divided in 128^3 cells. A monochromatic ionizing source, emitting photons with energy equal to 13.6 eV, is located at the centre of the box; the ionizing photon rate is $5 \times 10^{49}\,{\rm s}^{-1}$. The ionizing radiation is discretized in $N_{\rm p} = 10^7$ photon packets. The same source emits also an Lyα monochromatic radiation. As we want to construct spectra at a fixed distance from the source, we distribute the gas (H only, with density $n_{\rm H} = 1\,{\rm cm}^{-3}, N_{\rm H\,I} \sim 5 \times 10^{18}\,{\rm cm}^{-2}$ and temperature $T = 10^4$ K) in a sphere of radius $r_{\rm sph} = 15$ pc around the central source. Outside the sphere the density is set to zero, so that no interaction between radiation and gas takes place. The gas is initially neutral. Every simulation is carried out for a physical time of $t_{\rm sim} = 10^5$ yr. In our reference runs we have $N_{\rm out} = 50$ outputs and $N_{\rm em,l} = 100$ emissions of Lyα photons, each with $N_{\gamma,\rm l} = 10^4$ photons. Both the emissions and the outputs are dictated by the evolution of the ionization field. We will discuss the effect of a different choice for $N_{\rm em,l}, N_{\gamma,l}$ and $N_{\rm out}$ at the end of the section. In the following we present the results of our simulations for different choices of the dynamical state of the gas. The spectra shown are obtained integrating on all directions in order to achieve a better resolution, given the set of chosen parameters.

4.1 Static sphere

In this first test, the gas has no bulk velocity with respect to the central source. The top left-hand panel in Fig. 1 shows the spectra emerging from this configuration at times corresponding to volume-averaged ionization fractions $\chi_{\rm H\,II} = 0.3, 0.5, 0.8, 0.9, 0.99$, which could be regarded as spectra of the source observed at different times elapsed since the source switches on.

The spectra shown here and in the rest of the paper have been built as described in Section 3.3., i.e. collecting the Lyα photons escaping the system when $\chi_{\rm H\,II}$ falls in an interval $\Delta\chi_{\rm H\,II} = 0.02$ centred on the $\chi_{\rm H\,II}$ value selected for the output. The curve corresponding to $\chi_{\rm H\,II} = 0.99$ is instead a collection of the escaping photons which starts when $\chi_{\rm H\,II} = 0.98$ and ends at $t_{\rm sim}$. For the combination of parameters chosen for the tests, at $\chi_{\rm H\,II} < 0.3$ the number of escaped Lyα photons is not sufficient to build a spectrum and also for $\chi_{\rm H\,II} = 0.3$ the outgoing spectrum is very noisy. As expected, the spectra exhibit the two symmetric peaks characteristic of this configuration, although a direct, quantitative comparison with previous works (i.e. Dijkstra, Haiman & Spaans 2006) is not possible, as none included the effect of ionizing radiation. As the ionization increases, the peaks move towards $x = 0$ because Lyα photons encounter less and less H I atoms along their path. At the same time, the width of the peaks becomes smaller. In this scenario we do not see a spectrum peaked at $x = 0$ because the gas never gets completely ionized and, for a static configuration, also a little fraction of neutral gas far from the location of emission has a non-negligible optical depth for photons in the line centre.

4.2 Expanding and collapsing sphere

In a more interesting case we simulate a homogeneous spherical cloud that collapses or expands. In these tests we sample a velocity field, in the gas sphere, described by $V(r) = V_{\rm max}\, r/r_{\rm sph} + V_0$.

Initially we choose $V_{\rm max} = \pm 200\,{\rm km\,s}^{-1}$ and $V_0 = 0\,{\rm km\,s}^{-1}$. The resulting spectra extracted at the same ionization fractions as for the static case are shown in Fig. 1 with a positive and a negative value for $V_{\rm max}$ (top right-hand and centre left-hand panels, respectively). As

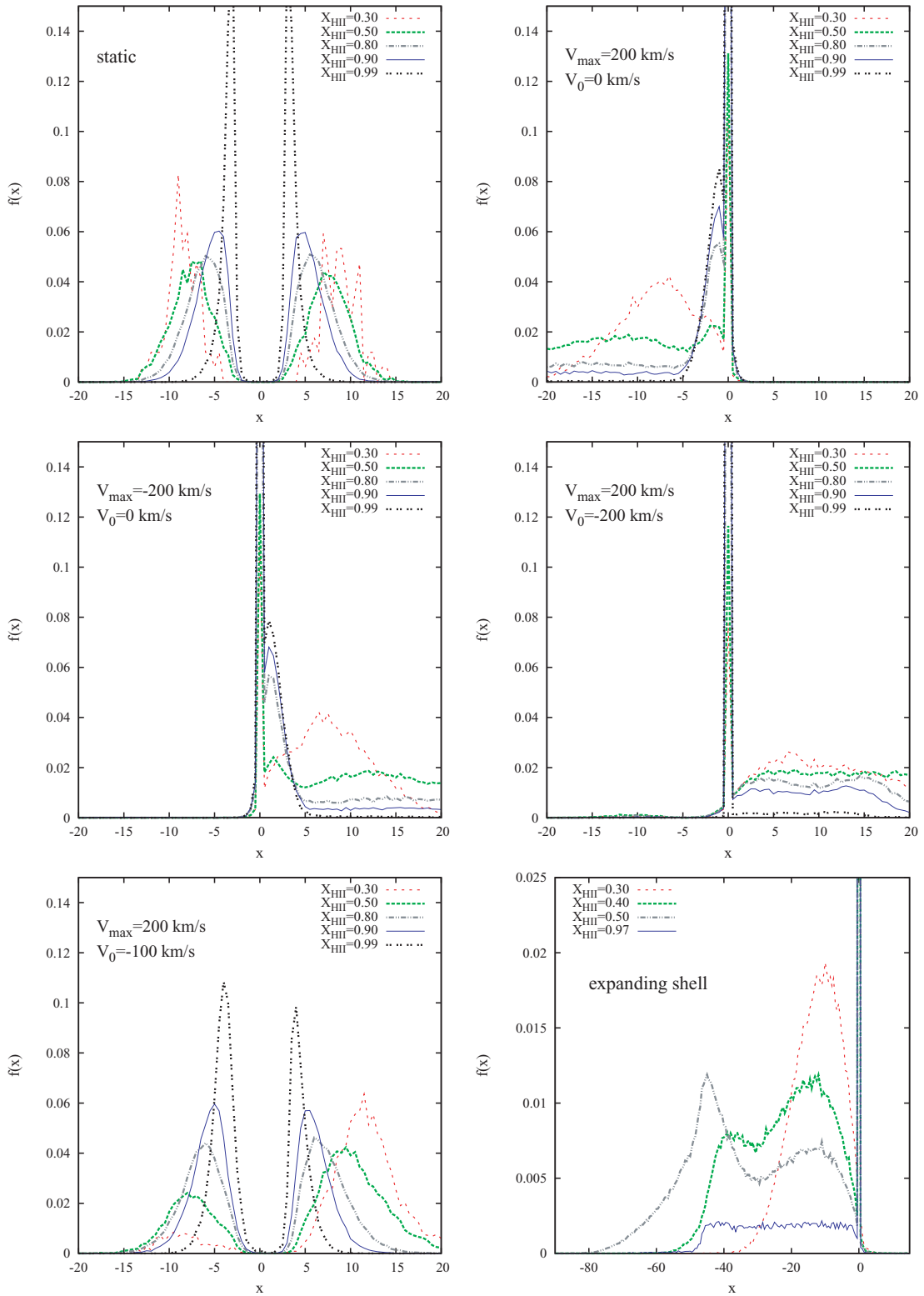

Figure 1. Spectra of Lyα outgoing radiation at times corresponding to ionization fractions $\chi_{\rm H II} = 0.3, 0.5, 0.8, 0.9, 0.99$ (with the exception of the bottom right-hand panel for which $\chi_{\rm H II} = 0.3, 0.4, 0.5, 0.97$). The dynamic condition of the gas is the following: static gas (upper left-hand panel), homogeneous spherical cloud expanding and collapsing with velocity increasing with distance from the source (upper right-hand and centre left-hand panels), homogeneous spherical cloud collapsing with velocity decreasing with distance from the source (centre right-hand and bottom left-hand panels), shell expanding at constant velocity (bottom right-hand panel).

expected, the plots show specular Lyα spectra, due to the opposite direction of the bulk motion. When the gas is expanding the outgoing radiation is on the red part of the spectrum, while it lays on the blue side when we consider negative values for the velocity. This happens because the photons are seen Doppler shifted according to the velocity of the atoms. This means that, if an atom has a positive velocity, in the atom rest frame a blue photon becomes a line centre photon and is easily blocked by the higher optical depth (compared to the optical depth in the wings). Thus, a photon can escape only if it is shifted by scattering to the red side of the line. Differently from the static case, here it is possible to have Lyα radiation at the central frequency $x = 0$ also when ionization is not complete. This is a consequence of the fact that, due to the Doppler effect, the line centre photons are seen in the atom rest frame as red (expanding gas) or blue (collapsing gas) photons, i.e. in the wing, and thus encounter a lower optical depth. In addition, the higher is the absolute value of the velocity the bigger is the shift, so when the continuum radiation ionizes the regions closer to the source (which have lower velocity and as a consequence a higher contribution to the opacity), the optical depth at the centre decreases significantly because the external neutral layers of gas (with a higher velocity) give only a minor contribution. As a result, as ionization proceeds, we start seeing an increasing emission at the central frequency. More specifically, the spectrum corresponding to $\chi_{\rm H\,II} = 0.3$ shows radiation at $x = 0$ and a residual in the red (blue) part of the spectrum for positive (negative) velocities. As ionization proceeds, the residuals become less pronounced and move towards the centre, while the central radiation becomes stronger. In the last spectrum, when the gas is 99 per cent ionized, there is still a residual because of the remaining neutral hydrogen fraction in the most distant regions of the gas sphere, where the photoionization rate is suppressed by geometrical dilution and by the residual inner opacity.

In the third case we consider a gas sphere collapsing with increasing velocity towards the centre. The centre right-hand panel of Fig. 1 shows Lyα profiles generated with a bulk motion characterized by $V_{\rm max} = 200$ km s^{-1} and $V_0 = -200$ km s^{-1}. These spectra are very similar to the ones obtained in the previous case, but as the absolute value of the velocities increases towards the centre, the residual blue part of the spectra is more spread. Note that also in this case the residual is reduced as ionization proceeds and the contribution to the opacity from the inner layers of gas is suppressed.

In the last case (Fig. 1, bottom left-hand panel) we consider a gas which is collapsing near the source while the outer shells are expanding, with $V_{\rm max} = 200$ km s^{-1} and $V_0 = -100$ km s^{-1}. The first Lyα spectrum (at $\chi_{\rm H\,II} = 0.3$) is dominated by photons in the blue part and just a residual is present on the red side. In fact, blue photons have a larger probability to escape because the ionization front has not yet propagated far enough to suppress the contribution to the Lyα gas opacity from the gas collapsing towards the source. As the front proceeds ionizing the neutral hydrogen with negative velocities (spectra at increasing $\chi_{\rm H\,II}$), the red part of the spectrum becomes stronger while the blue part is suppressed, until, in the configuration with $\chi_{\rm H\,II} = 0.99$, it is smaller than the red one. As in the other tests, the increment in the ionization degree reduces the number of scatterings, with the consequence of moving the two peaks towards the centre, increasing their height and reducing their width.

4.3 Expanding shell

In this section we examine the case of an Lyα source surrounded by an expanding shell, which has been extensively studied also by other authors (Ahn 2004; Hansen & Oh 2006; VSM06). Here, we are interested in the effects introduced on the Lyα spectrum by an ionizing source inducing a time evolution of the neutral gas in the shell. To simulate this configuration we have chosen a homogeneous density $n_{\rm H} = 15$ cm^{-3}, temperature $T = 10^4$ K, and radial velocity $V = 300$ km s^{-1}. All the gas is distributed within a shell of thickness 4 pc located at a distance of 10 pc from the source, while no gas is present outside the shell. The corresponding column density is $N_{\rm H\,I} \sim 2 \times 10^{20}$ cm^{-2}. To show the Lyα spectrum time evolution, we choose to plot the profiles corresponding to ionization fractions in the shell of $\chi_{\rm H\,II} = 0.30, 0.40, 0.50, 0.97$ (Fig. 1, bottom right-hand panel). For a better understanding of the spectral features, it is useful to discuss the possible different paths for an outgoing photon. Following VSM06 (see their fig. 12), we divide the outgoing photons in three different groups, depending on their scattering history.

(i) Backscattered photons: photons that, after scattering in the shell, travel inward across the empty space before crossing again the shell. As these photons undergo multiple scatterings with the gas, they can escape once they are shifted on the red side of the line where the optical depth of the expanding shell is smaller.

(ii) Diffused photons: all the photons which are diffused in the shell until they escape without backscattering. We expect these photons to contribute to a red bump in the spectra whose shift from the line centre and intensity will depend on the neutral gas density and on the shell velocity. Typically the frequency shift will be smaller than for backscattered photons as the number of scatters before escape is on average lower.

(iii) Directly escaped photons: photons that have no interaction with the gas and keep their initial frequency; in our case this group of photons will produce a peak at $x = 0$.

It is important to underline that every group has a different characteristic time for escaping. In fact, directly escaped photons travel the shortest path. On the other hand, diffused photons scatter in a volume smaller than the backscattered photons and thus escape faster; therefore the red bump associated to the diffused photons will typically appear before the feature produced by the backscattered photons.

Keeping in mind all the possible paths for Lyα photons, let us analyse the features in the spectra shown in the Fig. 1 (bottom right-hand panel). The first profile ($\chi_{\rm H\,II} = 0.3$) exhibits a peak on the red side of the central emission, due to the diffused photons, that, as already mentioned, escape faster than backscattered photons and can already been seen in the initial stages of the shell ionization. Directly escaped photons are present as well and their abundance increases with time. In the profile corresponding to an ionization degree of $\chi_{\rm H\,II} = 0.4$ we can clearly see that a secondary bump is forming at lower frequencies. At this stage of the evolution, the backscattering photons are starting to escape from the shell with a frequency that is more shifted respect to the other photons, as explained above. When the ionization degree is $\chi_{\rm H\,II} = 0.5$, the backscattering bump is visible and dominant on the red peak due to diffused photons. In the profile corresponding to $\chi_{\rm H\,II} = 0.97$ the ionization front has suppressed most of the neutral gas and only a negligible fraction of Lyα radiation interacts with the residual gas in the shell; the result is a small fraction of photons shifted on the spectrum's red side.

4.4 Effect of ionizing radiation

In the previous tests we have discussed how our time-dependent treatment of the Lyα radiation allows us to correctly establish the

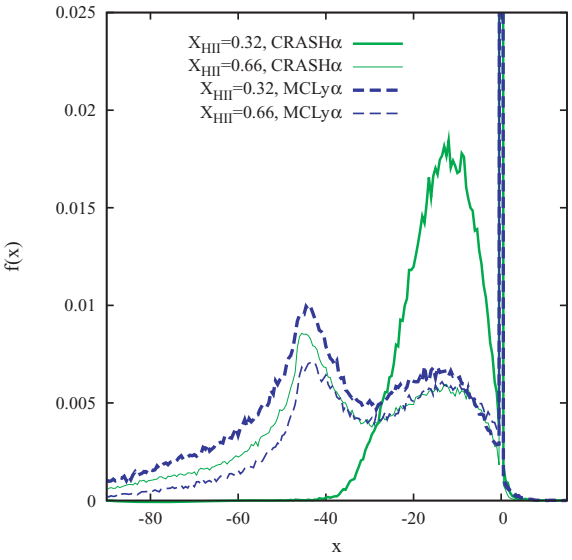

Figure 2. Comparison of Lyα spectrum obtained with MCLYα and CRASHα applied to the same gas distribution of an expanding shell. For the application of MCLYα a fixed gas configuration is used, while in our approach all the evolutionary stages are taken into account (see text for details).

appearance at different times of spectral features which are usually integrated in the emergent spectra predicted with time-independent formulations. Here we investigate further on the importance of the joint propagation of Lyα and continuum radiation, by comparing results from two different approaches to simulate the Lyα spectra. The first one, widely used in the literature, performs an Lyα radiative transfer on a gas configuration given as initial condition, which can be e.g. a constant density field or a snapshot of a numerical simulation. In this case, the gas configuration is kept constant throughout the entire Lyα radiative transfer and the Lyα spectra are built once all the Lyα photons have escaped the simulation volume. The other approach is the one described in this paper, i.e. starting from an initial gas configuration, the parallel propagation of continuum and line photons is followed and the Lyα spectra can be built at different times taking into full account the changes in the Lyα propagation due to the variations in the neutral gas distribution.

To show the impact of the two different approaches on the outgoing Lyα spectra, we consider the same configuration described in Section 4.3, i.e. an initial neutral expanding shell which is ionized by a central source emitting also Lyα photons. We compare the spectra obtained with CRASHα at the times when the gas configuration is characterized by a mean ionization fraction inside the shell of $\chi_{\rm H\,II} = 0.32$ and 0.66, to those obtained running MCLYα on the same gas configurations. While with MCLYα the spectra are built by integrating over the Lyα photons once they have all escaped the fixed H I distribution, the CRASHα algorithm allows us to account for the impact on the emergent spectra of the ionization history which led to those configurations. The results are shown in Fig. 2.

A substantial difference is clearly visible in the spectra corresponding to $\chi_{\rm H\,II} = 0.32$. The Lyα spectrum simulated by MCLYα is characterized by two bumps associated with the diffused and backscattered photons. A very different profile is obtained with CRASHα, where no backscattered photon has escaped at this time and only the single red peak corresponding to the diffused photons is present. As already underlined in Section 4.3 the absence of backscattered photons is due to their larger escaping time. The profiles corresponding to $\chi_{\rm H\,II} = 0.66$ are much more similar, because at this stage a significant fraction of the backscattered photons had enough time to escape the shell. Nevertheless, there is still a difference in the amplitude of the peak at $x = 0$ and of the bumps from the backscattered photons, which are also slightly more shifted. This difference is due to the memory of Lyα photons emitted in the previous stages of the source activity, when $\chi_{\rm H\,II} < 0.6$. In the MCLYα treatment all the emitted Lyα photons see the same mean shell opacity and the probability to have a direct escape is significantly higher then in the CRASHα run, in which the Lyα photons see on average a larger shell opacity. As a consequence, the fraction of photons with $x = 0$ in CRASHα is smaller and, at the same time, the photons that have remained trapped for a longer time exhibit a larger amplitude of the spectra and a larger shift to the red side of the central frequency. The time elapsed between the two spectra considered above is only about 100 yr. The time interval in which deviations from the 'instantaneous picture' are significant is thus too small to allow observations to capture these stages. However, the example is useful to illustrate the relevant features and advantages of our approach. Furthermore the deviations found could affect the gas state, e.g. its spin temperature, independently from their observational detectability in the spectra.

A similar test has been performed to infer the observability of the deviations in the spectra on larger scales. In this case we use a simulation box of 200 kpc on a side and a photoionization rate of the central source $\dot{N}_\gamma = 10^{54}\ {\rm s}^{-1}$. In this test the gas is distributed in a sphere of radius $r_{\rm sph} = 70$ kpc, with density $n_{\rm H} = 0.01\ {\rm cm}^{-3}$ (corresponding to $N_{\rm H\,I} \sim 2 \times 10^{21}\ {\rm cm}^{-2}$), while we keep the temperature $T = 10^4$ K; we also assume a velocity field corresponding to a Hubble expansion with $H = 790\ {\rm km\ s}^{-1}\ {\rm Mpc}^{-1}$. The simulation is carried out for a physical time of $t_{\rm sim} = 10^8$ yr. In this case (Fig. 3) the first spectrum is captured at the time $t = 4.0 \times 10^6$ yr (corresponding to a mean ionization fraction of $\chi_{\rm H\,II} = 0.24$) and the second at the time $t = 8.3 \times 10^6$ yr ($\chi_{\rm H\,II} = 0.40$). While the MCLYα profile in the left-hand panel of Fig. 3 is characterized by a large red bump and a small blue one, with the CRASHα approach we find a lower fraction of photons escaping with blue frequencies and a larger red bump which is slightly shifted on redder frequencies. This effect results from keeping memory of the ionization history, since we take into account that before reaching the observed gas configuration most of the Lyα photons have been trapped on the boundary of the growing ionized region. The integrated optical depth along the full path travelled before escaping is therefore larger respect to the one computed in the MCLYα approach. This effect is also visible in the right-hand panel of Fig. 3, where a larger redshift is present. In this case a larger fraction of trapped photons are now free to escape and the shift is more evident.

The major result of these tests is that the emerging spectra keep memory of the ionization history which generates a given observed configuration and, to properly account for this effect, the self-consistent joint evolution of line and ionizing continuum radiation followed by our scheme is necessary. The extent of the difference between the two methods depends on the particular case considered, but it can be substantial and can thus affect the physical interpretation of the problems at hand. In a forthcoming study we will investigate in more detail which are the objects/configurations for which the ionization effects are expected to be relevant in shaping the observed Lyα spectrum.

In addition, the time evolution that builds up the Lyα radiation field can be important when calculating the impact of such radiation on gas properties like the spin temperature, which is relevant for the prediction of the observability of 21-cm emission from neutral

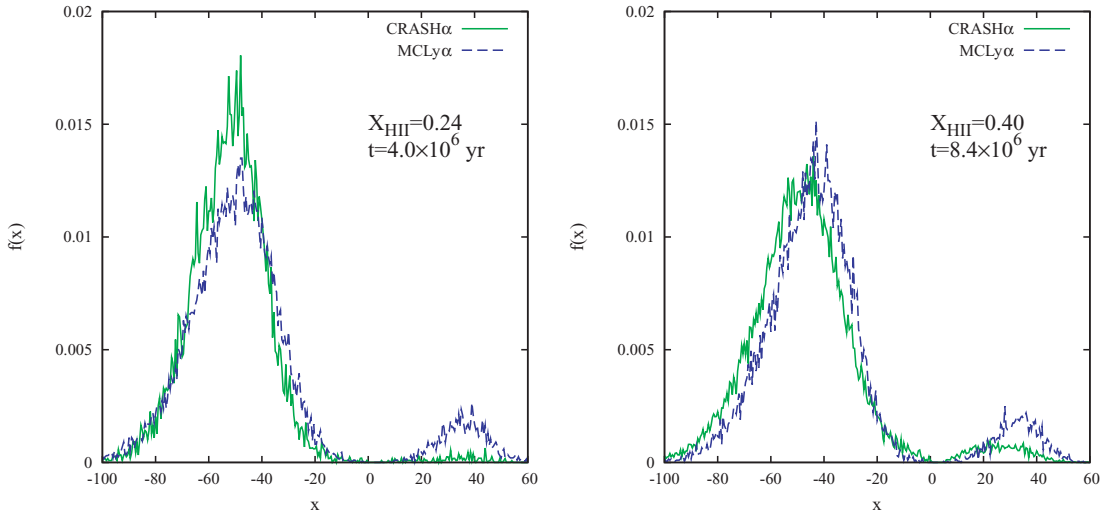

Figure 3. Comparison of Lyα spectrum obtained with MCLYα and CRASHα applied to the same gas distribution of an expanding sphere. The left-hand (right-hand) panel shows Lyα profiles at $t = 4.0 \times 10^6$ yr (t = 8.4×10^6 yr). See text for more details.

hydrogen at high redshift. We plan to include the computation of these effects in a forthcoming extension of the code.

4.5 Dependence on input parameters

In this section we investigate the dependence of the final spectra on the parameters $N_{\rm em,l}, N_{\gamma,\rm l}$ and $N_{\rm out}$ defined in Sections 3.1 and 3.3. The convergence tests presented are performed by adopting the same conditions of the static case (see Section 4.1).

First, we compare spectra built by integrating over the full simulation time, i.e. we set $N_{\rm out} = 1$. We have done several runs varying the number of Lyα emissions ($N_{\rm em,l} = 2, 10, 50, 100$) and setting $N_{\gamma,\rm l} = 10^4$. Lyα photons are emitted according to equation (6), i.e. at regular ionization intervals. For $N_{\rm em,l} = 2$, the two emissions are performed at the beginning and once the ionization degree has become stationary. The results are shown in the top left-hand panel of Fig. 4. From an inspection of the figure it is clear that the two emissions are not accurate enough to properly describe the emergent Lyα spectrum. This is a consequence of the method described in Section 3.1 for weighting the contribution to the spectrum from photons emitted at different steps. In fact, as the time between the two emissions is large, the weight assigned to the photons of the second (and last) emission is so large that the contribution from the photons of the first emission is negligible. Moreover, at the time of the second emission ionization is almost complete and as a consequence the spectrum has two thin peaks very close to the central frequency and shows no large frequency shift due to scattering in a gas with larger opacity. So, in this case the outgoing spectrum is the result of Lyα transfer in an almost ionized sphere and the stages through which the gas reached such configuration are completely neglected. As the number of emissions is increased, the accuracy improves and convergence is reached when $N_{\rm em,l} > 50$.

We have then checked convergence of instantaneous (versus integrated) spectra, setting $N_{\rm out} = 10$ and performing again four runs with different numbers of Lyα emissions ($N_{\rm em,l} = 2, 10, 50$ and 100) and $N_{\gamma,\rm l} = 10^4$. Fig. 4 displays two sets of spectra, each corresponding to a fixed $\chi_{\rm H\,II}$ value: 0.4 (top right-hand panel) and 0.7 (bottom left-hand panel). Effectively, the spectrum corresponding to $N_{\rm em,l} = 2$ is built only with photons from the first emission, as the second is performed when $\chi_{\rm H\,II} > 0.7$. At $\chi_{\rm H\,II} = 0.4$ the spectra are all very similar because the gas opacity is sufficiently high to trap Lyα photons and those emitted close to the time when the spectrum is built are still scattering in the gas. On the contrary, as ionization proceeds, photons emitted at later times encounter less neutral hydrogen and escape more easily, and their contribution to the outgoing spectrum increases. As a consequence, the case with $N_{\rm em,l} = 2$, when Lyα photons have been emitted only at the beginning of the simulation, displays a broader and more shifted profile.

Finally, we use different values of $N_{\gamma,\rm l} = 10^3, 10^4, 10^5$, with $N_{\rm em,l} = 100$ and $N_{\rm out} = 50$, to determine the smallest number of Lyα photons needed in each emission in order to achieve convergence. In the bottom right-hand plot we show Lyα profiles corresponding to an ionization fraction of $\chi_{\rm H\,II} = 0.7$. As expected, the increasing number of Lyα photons in every emission produces a smoother profile. We find that, for the configuration considered, the emissions characterized by 10^3 photons are not accurate enough, and at least 10^4 photons per emission are needed.

5 SUMMARY

In this paper we have presented CRASHα, the first radiative transfer code for cosmological application that follows the parallel propagation of Lyα and continuum photons. Since Lyα propagation is dominated by resonant scattering with neutral gas, the effect of a rapid change in the degree of gas ionization can affect the features of the emerging Lyα spectrum. To investigate this issue, we have developed in the continuum radiative transfer code CRASH (Ciardi et al. 2001; Maselli et al. 2003; Maselli & Ferrara 2005; Maselli et al., in preparation), a new algorithm to follow the propagation of Lyα photons through a gas configuration while it is changed by ionizing radiation.

In order to perform the implementation, it has been necessary to introduce the time evolution for Lyα propagation, a feature commonly neglected in line radiative transfer codes. This is a crucial aspect because, due to the resonant scattering nature of Lyα transfer in a neutral medium, Lyα radiation can remain trapped for a substantial fraction of the simulation lifetime before being able to propagate away from its emission site, while the propagation time of the ionization front can be much shorter. Another challenge of the implementation has been to reduce the computation

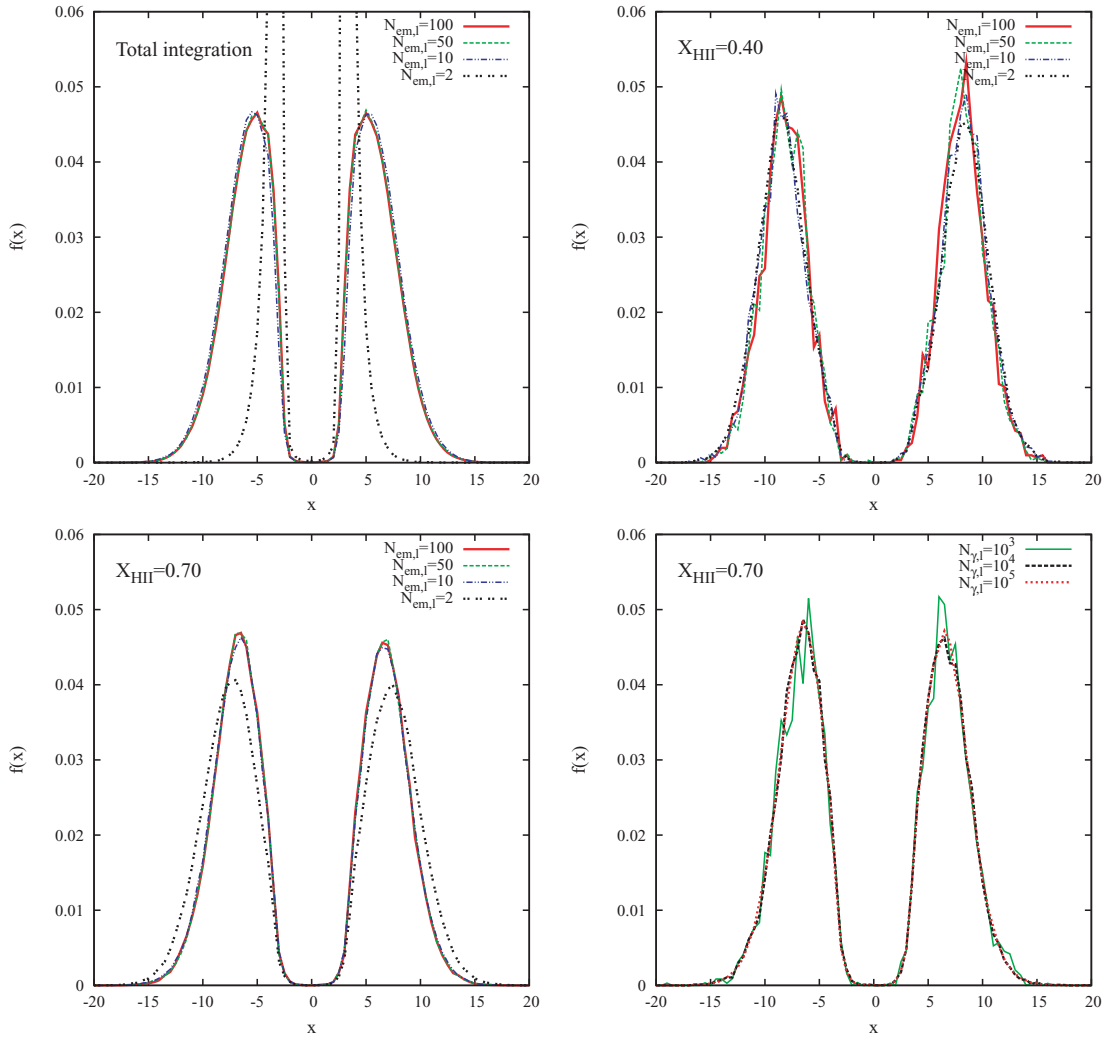

Figure 4. Effect of the input parameters on the final spectra. The top left-hand plot shows the Lyα spectra integrated over the full simulation time ($N_{\rm out} = 1$) using a different number of Lyα emissions, $N_{\rm em,l}$, and $N_{\gamma,\rm l} = 10^4$. The top right-hand and bottom left-hand plots show the instantaneous spectrum at $\chi_{\rm H\,II} = 0.4$ and 0.7 respectively, with the same values of $N_{\rm em,l}$ and $N_{\gamma,\rm l}$. Finally, the bottom right-hand plot shows a case with $N_{\rm em,l} = 100, N_{\rm out} = 50$ and a spectrum at $\chi_{\rm H\,II} = 0.7$ with different values of $N_{\gamma,\rm l}$.

time for the Lyα scattering. In fact, to correctly model the Lyα propagation every single scattering should be followed. As this would require prohibitively large computational times, we have used a statistical approach to the Lyα treatment. We have compiled tables using MCLYα (VSM06) to describe the physical characteristics of a photon escaping from a gas cell where it was trapped by scattering as a function of the temperature and density of the gas as well as of the incoming photon frequency. The tables are called within CRASHα. With this statistical approach we experience a drastic reduction of the computational time and, at the same time, an excellent agreement with the full Lyα radiative transfer computations.

We have discussed the details of the code implementation and tested it for several gas configurations, including static spherical gas distribution, expanding and collapsing spheres and expanding shell. For all the configurations analysed, CRASHα reproduces emerging spectra with the qualitative features expected from theoretical models and discussed previously in the literature, while a more quantitative comparison has not been feasible as CRASHα is the first code which couples the continuum and line transfer. With this implementation, it has also been possible to investigate how the line shape of the emergent spectra evolves with the gas ionization. Although the specific results depend on the geometry of the gas and on the velocity field, common trends are found. The main results can be summarized as follows.

(i) While ionization proceeds the peaks on the blue/red side of the line centre move closer to the central frequency, getting thinner and higher, as expected for a gas configuration with progressively decreasing optical depth. Depending on the gas configuration (e.g. in case of an expanding shell), more complex features arise that can be associated to the different paths followed by the Lyα photons before escaping.

(ii) The emerging spectra keep memory of the ionization history which generates a given gas configuration.

(iii) The novel approach to Lyα transfer developed in CRASHα allows us to resolve the emergence of different spectral features at different times during the evolution of the ionization field. Features emerging on different time-scales are typically associated to the various paths travelled by the photons before escaping.

(iv) A comparison between our new algorithm to follow the propagation of Lyα photons and a full line radiative transfer shows an excellent agreement for different gas configurations and an enormous gain in computational speed.

In order to account for the effects discussed above a self-consistent joint evolution of line and ionizing continuum radiation as implemented in CRASHα is necessary. A comparison between the results from our code and from Lyα scattering alone on a fixed density field shows that the extent of the difference between the emerging spectra depends on the particular configuration considered, but it can be substantial and can thus affect the physical interpretation of the problem at hand.

A detailed discussion on which are the objects/configurations for which the ionization effects are expected to be relevant in shaping the observed Lyα spectrum is deferred to a forthcoming paper. Nevertheless, we have here discussed two specific test configurations for which the coupling of continuum and line radiation would be necessary in order to recover correctly the emergent profile. These differences are due to the time evolution feature introduced in CRASHα for Lyα photons which allows us to keep track of the ionization history imprint on Lyα profiles for the first time in the literature.

The time evolution that builds up the Lyα radiation field can be furthermore important when calculating the impact of such radiation on gas properties like the spin temperature, relevant to predict the observability of 21-cm radiation from the early Universe. In a forthcoming extension of the code CRASHα, we plan to include the self-consistent calculation of the impact of the Lyα radiation on the gas temperature, together with the contribution to the Lyα radiation from recombinations occurring in the gas.

ACKNOWLEDGMENTS

The authors thank Anne Verhamme and Daniel Schaerer for providing the last version of the code MCLYα and for their comments. They are also thankful to Andrea Ferrara for stimulating discussions and sharp comments on the draft. AM is supported by the DFG Priority Programme 117.

REFERENCES

Adams T. F., 1972, ApJ, 174, 439
Ahn S. H., 2004, ApJ, 601, L25
Ahn S. H., Lee H. W., Lee H. M., 2000, J. Korean Astron. Soc., 33, 29
Ahn S. H., Lee H. W., Lee H. M., 2001, ApJ, 554, 604
Avery L. W., House L. L., 1968, ApJ, 152, 493
Barkana R., Loeb A., 2005, ApJ, 626, 1
Cantalupo S., Porciani C., Lilly S. J., Miniati F., 2005, ApJ, 628, 61
Chen X., Miralda-Escudé J., 2008, ApJ, 684, 18
Chuzhoy L., Zheng Z., 2007, ApJ, 670, 912
Ciardi B., Madau P., 2003, ApJ, 596, 1
Ciardi B., Salvaterra R., 2007, MNRAS, 381, 1137
Ciardi B., Ferrara A., Marri S., Raimondo G., 2001, MNRAS, 324, 381
Dijkstra M., Haiman Z., Spaans M., 2006, ApJ, 649, 14
Dawson S., Rhoads J. E., Malhotra S., Stern D., Wang J., Dey A., Spinrad H., Jannuzi B. T., 2007, ApJ, 671, 1227
Fan X. et al., 2006, ApJ, 132, 117
Field G. B., 1958, Proc. IRE, 46, 240
Field G. B., 1959, ApJ, 129, 536
Gould A., Weinberg D. H., 1996, ApJ, 468, 462
Hansen M., Oh S. P., 2006, MNRAS, 367, 979
Harrington J. P., 1973, MNRAS, 162, 43
Hu E., Cowie L. L., McMahon R. G., 1998, ApJ, 502, L99
Hu E., Cowie L. L., McMahon R. G., Capak P., Iwamuro F., Kneib J.-P., Maihara T., Motohara K., 2002, ApJ, 568, 75
Hu E., Cowie L. L., Capak P., McMahon R. G., Hayashino T., Komiyama Y., 2004, AJ, 127, 3137
Iye M. et al., 2006, Nat, 443, 186
Kashikawa M. et al., 2006, ApJ, 648, 7
Kobayashi M. A. R., Kamara H., 2004, ApJ, 600, 564
Kodaira K. et al., 2003, PASJ, 55, 17
Loeb A., Rybicki G. B., 1999, ApJ, 524, 527
Maselli A., Ferrara A., 2005, MNRAS, 364, 1429
Maselli A., Ferrara A., Ciardi B., 2003, MNRAS, 345, 379
Murayama T. et al., 2007, ApJS, 172, 523
Neufeld D. A., 1990, ApJ, 350, 216
Osterbrock D. E., 1962, ApJ, 135, 195
Partridge R. B., Peebles J. E., 1967, ApJ, 147, 868
Pelló R., Richard J., Schaerer D., Le Borgne J.-F., Kneib J.-P., Hempel A., 2007, Rev. Mex. Astron. Astrofis., 29, 132
Rhoads J. E., Malhotra S., 2001, ApJ, 563, 5
Rhoads J. E. et al., 2003, AJ, 125, 1006
Semelin B., Combes F., Baek S., 2007, A&A, 474, 365
Stark D. P., Ellis R. S., Richard J., Kneib J.-P., Smith G. P., Santos M. R., 2007, ApJ, 663, 10
Stern D., Yost S. A., Eckart M. E., Harrison F. A., Helfand D. J., Djorgovski S. G., Malhotra S., Rhoads J. E., 2005, ApJ, 619, 12
Taniguchi Y. et al., 2005, PASJ, 57, 165
Tasitsiomi A., 2006, ApJ, 645, 792
Verhamme A., Schaerer D., Maselli A., 2006, A&A, 460, 397 (VSM06)
Wouthuysen S. A., 1952, AJ, 57, 31
Zheng Z., Miralda-Escudé J., 2002, ApJ, 578, 33

APPENDIX A: TABLES FOR LYα SCATTERING

Following the single scatterings of each Lyα photon can be extremely expensive; in order to avoid it we have built tables by using a statistical approach that allows us to retrieve the frequency of the outgoing photon, $x_{\rm out}$, and the time interval for which the photon is trapped in the gas by the scatterings, $t_{\rm scatt}$, given the frequency of the incoming photon, $x_{\rm in}$, the gas temperature, $T_{\rm cell}$, and optical depth, $\tau_{\rm cell}$, of the cell where the scattering takes place. We adopt the opacity at line centre to characterize the optical depth of the gas in a cell. Note that the frequencies are always meant in the comoving frame.

The tables are compiled in the following way. Given a value for the input parameters ($T_{\rm cell}$, $\tau_{\rm cell}$ and $x_{\rm in}$), we run the MCLYα code several times (the results converge when 10 000 Lyα photons are emitted) to obtain values for $x_{\rm out}$ and $t_{\rm scatt}$ which are then binned in distribution functions. The $x_{\rm out}$ distribution is binned using regular intervals of 0.5. For $t_{\rm scatt}$ we adopt equally spaced logarithmic bins of 0.014. It is important to note that the value of $t_{\rm scatt}$, which depends on the distance travelled by the photon, is linked to the size of the cell. Thus, the tables are compiled for a reference cell size, $d_{\rm c,ref}$, but anytime they are accessed by CRASHα, the value of $t_{\rm scatt}$ obtained needs to be linearly rescaled for the actual cell dimension, $d_{\rm c}$. The ranges that the tables cover are:

(i) temperature: $10 \leq T \leq 10^5$ K;
(ii) optical depth: $1 \leq \tau \leq 10^6$;
(iii) frequency: $-100 \leq x \leq 100$.

An example of $x_{\rm out}$ and $t_{\rm scatt}$ distributions is given in Figs A1 and A2. Fig. A1 shows the distribution of $x_{\rm out}$ for $T_{\rm cell} = 10^4$ K, $\tau_{\rm cell} = 10^6$ and different values of $x_{\rm in}$($x_{\rm in} = 20$, 30 and 40). Fig. A2 shows how the $t_{\rm scatt}$ distribution changes for different values of the optical depth, $\tau_{\rm cell} = 10^4, 10^5, 10^6$; here we fixed $T_{\rm cell} = 10$ K and $x_{\rm in} = 0$.

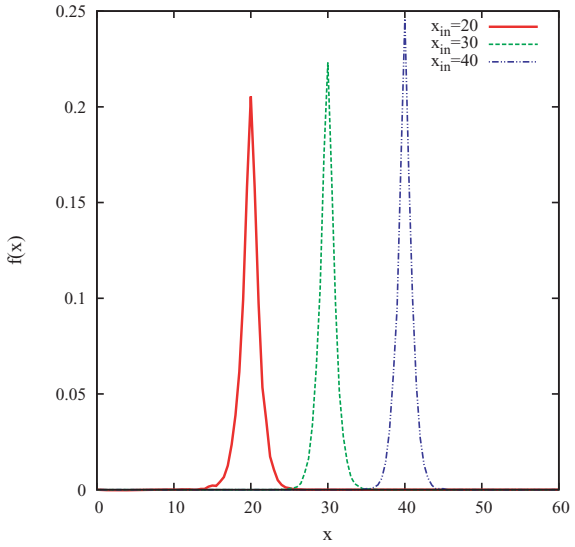

Figure A1. Distribution of photon outgoing frequencies generated by multiple scatterings inside a cubic cell with $T_{\rm cell} = 10^4$ K and $\tau_{\rm cell} = 10^6$ for an incoming photon frequency of $x_{\rm in} = 20$ (solid line), 30 (dashed line) and 40 (dash–dotted line).

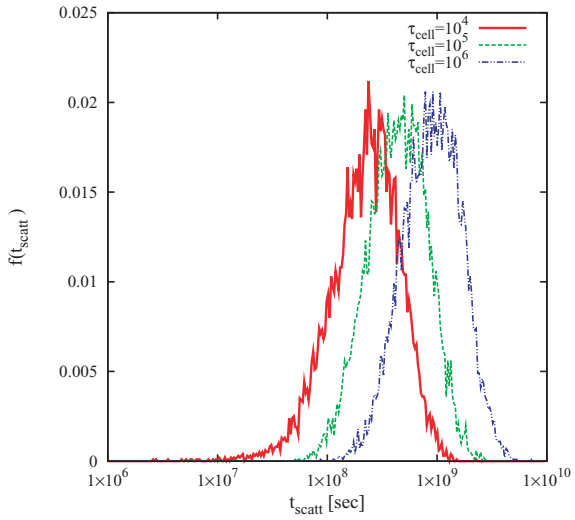

Figure A2. Distribution of the time that a photon with $x_{\rm in} = 0$ spends in a cubic cell with $T_{\rm cell} = 10$ K and an optical depth $\tau_{\rm cell} = 10^4$ (solid line), 10^5 (dashed line) and 10^6 (dash–dotted line).

The above tables are accessed by CRASHα in the following way. If $T_{\rm cell}$, $\tau_{\rm cell}$ and $x_{\rm in}$ are within the range covered by the tables, the distributions for $t_{\rm scatt}$ and $x_{\rm out}$ are calculated by a linear interpolation and then the value used in CRASHα for $t_{\rm scatt}$ and $x_{\rm out}$ is obtained by MC sampling the interpolated distributions. The interpolation scheme for $t_{\rm scatt}$ is as follows. As a first step, the values of temperature T_1 and T_2 closest to $T_{\rm cell}$ for which $T_1 \leq T_{\rm cell} < T_2$ are found. The same is done for the optical depths τ_1 and τ_2, and the frequencies x_1 and x_2. The weights to be assigned to each value are derived by linear interpolation. As an example we can consider a simple 1D case, with linear interpolation only on temperatures. In this case, $t_{\rm scatt} = w_{T_1} t_{\rm scatt}(T_1) + w_{T_2} t_{\rm scatt}(T_2)$, where the weights are $w_{T_1} = (T_2 - T_{\rm cell})/\Delta T$ and $w_{T_2} = (T_{\rm cell} - T_1)/\Delta T$, with $\Delta\, T = T_2 - T_1$. The same procedure, extrapolated in three dimensions, produces

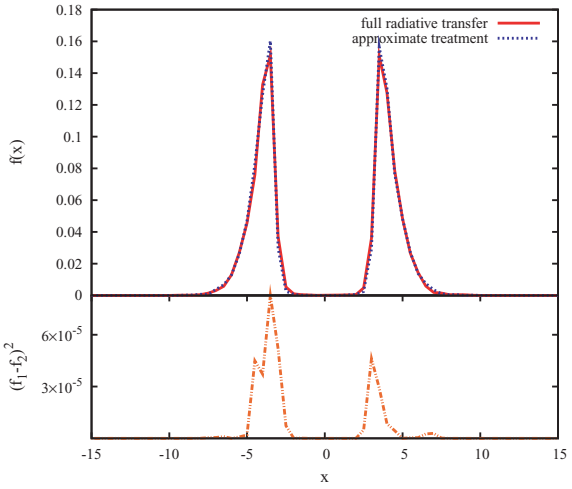

Figure A3. The upper panel shows the predicted Lyα frequency distribution for monochromatic line radiation escaping from a gas with temperature $T = 8000$ K and optical depth $\tau = 10^6$. The dotted (solid) line indicates the results for the approximate (full radiative transfer) treatment using tables build with 10 000 photons. The difference between the two distributions is shown in the bottom panel.

a distribution of $t_{\rm scatt}$ that will be randomly sampled in CRASHα. The interpolation for $x_{\rm out}$ follows the same steps, after a shift in the frequency space has been performed to assure that the correct distribution is obtained and no spurious peak forms. To understand how the $x_{\rm out}$ interpolation works an easy example can be useful. Let us assume that our purpose is to reproduce the dashed profile centred in $x = 30$ (Fig. A1) starting from the two profiles at $x = 20$ and 40. If the interpolation were performed bin by bin without any previous shift (e.g. the bin [19.5–20[of the solid curve with the bin [39.5–40[of the dash–dotted curve, and similarly for all the bins), the result would be two smaller peaks centred at $x = 20$ and 40, rather than one centred at $x = 30$. To perform a correct interpolation we need to centre the solid and dash–dotted profiles on $x = 30$ and then interpolate.

To check the validity of our approach, we have compared the results from the full radiative transfer treatment (using MCLYα) with a case in which the tables were used. In Fig. A3 the distribution in frequency of 10 000 Lyα photons escaping from a gas with temperature $T = 8000$ K, optical depth $\tau = 10^6$ and frequency $x = 0$ is shown. The dotted (solid) line in the upper panel indicates the results for the approximate (full radiative transfer) treatment using tables built with 10 000 photons. In the bottom panel the difference between the two distributions is plotted, showing an excellent agreement, which is found also for different initial conditions. We perform the same check with a more complex gas distribution using the expanding shell described in Section 4.3. As the final spectrum is expected to have a wider frequency distribution, this test is performed to check the accuracy of the $x_{\rm out}$ interpolation at larger frequency shifts. The results are shown in Fig. A4; for both profiles we have used 400 000 photons. Also in this case an excellent agreement is found.

We perform a final test in which we follow the evolution of an ionization field, tracing each Lyα scattering and then we compare the results with the CRASHα approach. The initial conditions are the same described in Section 4.1 but with a lower gas density, $n_{\rm H} = 0.01$ cm^{-3}, to ensure that the former computation is not prohibitively expensive. Fig. A5 shows the spectra of escaped photons when the averaged ionization degree is ∼50 per cent. Since the profiles are

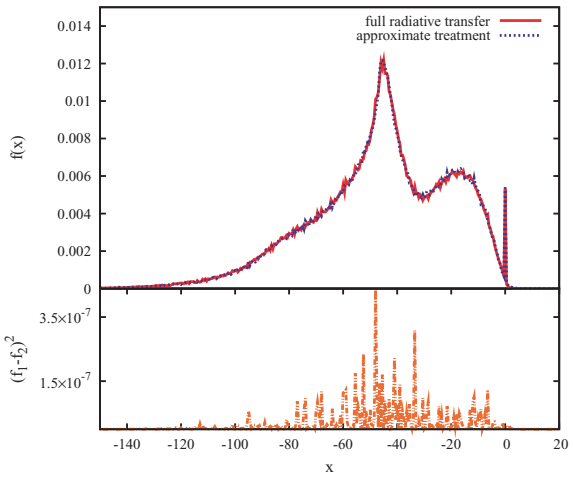

Figure A4. As Fig. A3 but for a gas configuration resembling a shell with temperature $T = 10^4$ K and column density $N_{\rm H\,I} = 2 \times 10^{20}$ cm^{-2} expanding with an uniform radial velocity $V = 300$ km s^{-1}. The dotted (solid) line in the upper panel indicate the results for the approximate (full radiative transfer) treatment using tables build with 400 000 photons. The difference between the two distributions is shown in the bottom panel.

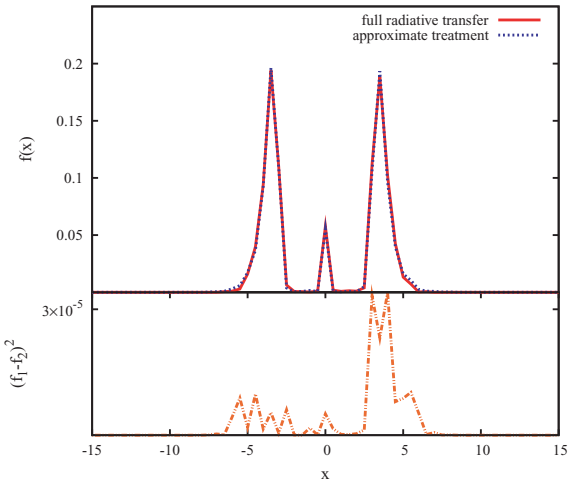

Figure A5. Comparison of Lyα spectra obtained with a full Lyα treatment, following each scattering, and with CRASHα approach. The profiles refer to a static sphere with temperature $T = 10\,000$ K, gas density $n_{\rm H} = 0.01$ cm^{-3} and radius $r_{\rm sph} = 15$ pc, when the averaged ionization degree is about 50 per cent. The difference between the two distributions is shown in the bottom panel.

very similar, we conclude that our approach is able to reproduce with a high accuracy both the frequency distribution and the time evolution of Lyα photons. In addition, the use of the tables allows an enormous gain in computational speed.

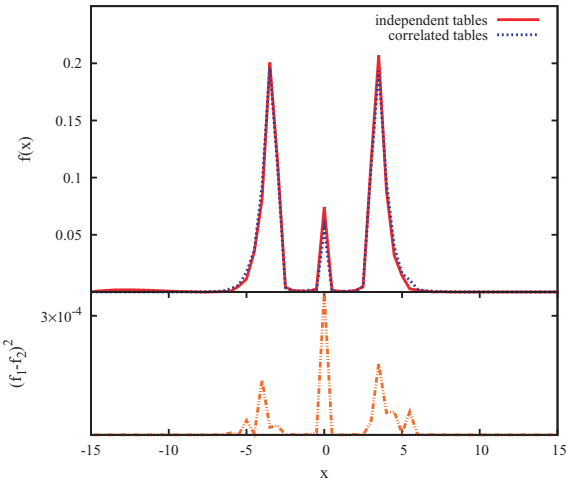

Figure A6. Comparison of Lyα spectra obtained extracting $x_{\rm out}$ and $t_{\rm scatt}$ using uncorrelated 1D tables, or correlated 2D ones. The profiles refer to a static sphere with temperature $T = 10\,000$ K, gas density $n_{\rm H} = 0.01$ cm^{-3} and radius $r_{\rm sph} = 15$ pc, when the averaged ionization degree is about 50 per cent. The difference between the two distributions is shown in the bottom panel.

As the changes in the gas properties during a simulation can be drastic, sometimes the values $\tau_{\rm cell}$ and $x_{\rm in}$ can fall outside the range covered by the tables (we do not expect $T_{\rm cell}$ to fall outside the range). In these cases we perform an extrapolation of the existing tables. More in particular, for $\|x_{\rm in}\| > 100$ we use the same distributions derived for $\|x_{\rm in}\| = 100$. This is a good approximation as at these frequencies the cross-section is small and Lyα scattering rare. The extrapolation for the optical depth works differently. If $\tau_{\rm cell} < 1$ no interaction takes place and the photon propagates freely. If $\tau_{\rm cell} > 10^6$ we divide the cell into 2^{3n} subcells (where n is the number of divisions performed) until each subcell has an optical depth $<10^6$. At this point, every subcell is treated as a single cell.

It is worthwhile noting that using two separate extractions for $x_{\rm out}$ and $t_{\rm scatt}$ imply that the frequency and time distribution are independent. This is not always true. Since in most cases of interest the approximation introduced induces only a very weak effect on the results, we typically assume that this correlation can be neglected. Nevertheless, as CRASHα is designed to work under conditions as general as possible, we have also implemented the possibility to use correlated 2D tables, which perform a single extraction of $x_{\rm out}$ and $t_{\rm scatt}$. We repeat the last test using both approaches and we show the results in Fig. A6. It is clear that the correlation has indeed a minor effect.

This paper has been typeset from a TEX/LATEX file prepared by the author.